THE EFFECTS OF PRECIPITATION ON RADAR
TARGET IDENTIFICATION AND IMAGING

D. B. Hodge

The Ohio State University

ElectroScience Laboratory

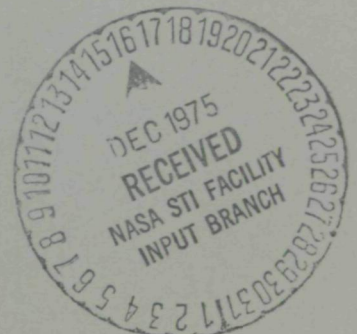Department of Electrical Engineering
Columbus, Ohio 43212

TECHNICAL REPORT 2374-19

November 1975

National Aeronautics and Space Administration
Goddard Space Flight Center
Greenbelt, Maryland 20771

NOTICES

When Government drawings, specifications, or other data are used for any purpose other than in connection with a definitely related Government procurement operation, the United States Government thereby incurs no responsibility nor any obligation whatsoever, and the fact that the Government may have formulated, furnished, or in any way supplied the said drawings, specifications, or other data, is not to be regarded by implication or otherwise as in any manner licensing the holder or any other person or corporation, or conveying any rights or permission to manufacture, use, or sell any patented invention that may in any way be related thereto.

THE EFFECTS OF PRECIPITATION ON RADAR
TARGET IDENTIFICATION AND IMAGING*

D. B. Hodge

ABSTRACT. The properties of precipitation which will influence
radar system design are discussed. The spatial characteristics
of rainfall and the sizes and shapes of raindrops are de-
scribed. The dielectric behavior of water is combined with
these characteristics to determine the effects of rain on
electromagnetic waves. These effects include: absorption,
scatter, noise emission, phase shift, and depolarization.

******

The treatment of microwave propagation in the troposphere
can be a difficult task even in the case of a clear atmosphere.
The presence of precipitation along a propagation path adds even
further complication to this task. This fact is primarily due
to the extreme spatial and temporal variability of precipitation.
Fortunately, the basic interactions between electromagnetic waves
and precipitation are well understood and may be quantitatively
described with a reasonable degree of certainty. It is the fine
scale spatial and temporal statistics of precipitation which
are not known adequately to permit detailed statistical de-
scriptions of these interactions at the present time.

The objective of this tutorial paper is to provide the radar design engineer with enough basic, quantitative information that he may establish realistic bounds on the performance of a given radar system in the presence of precipitation. A great deal of information concerning this topic is available in the literature, and much of this information has been collected and summarized at the recent IUCRM Colloquium on the Fine Scale Structure of Precipitation and Electromagnetic Propagation, Nice, France, October, 1973. The entire proceedings of this meeting, including review papers, are readily available in Reference 1 for further details covering these topics.

The likelihood of the occurence of precipitation is highly variable and may be strongly dependent upon the climatic region of the earth, the season of the year, the time of day, and even, in some cases, the local topography. Nevertheless, one may expect precipitation at many points on the earth's surface more than 5 per cent of the time and, of course, considerably higher percentages of time for the occurrence of precipitation along extended propagation paths. Therefore, if the impact of precipitation on system performance is significant, the reliability of the system may be impaired beyond tolerable limits.

For our purposes, precipitation may be divided into three types: rain, snow, and hail. Rain consists of liquid water drops which may be supercooled if they are carried above the 0°C isotherm by updrafts. These liquid water droplets interact strongly with propagating EM waves in the microwave and millimeter wavelength portions of the spectrum; these interactions include attenuation, phase shift, scattering, depolarization, and noise emission. It must be emphasized that these effects are distinct from the effects of water vapor, i.e., water in its gaseous form, which is present in the clear atmosphere. Snow and hail are normally forms of solid water which do not interact strongly with EM waves in this portion of the spectrum. One exception is, however, the case of melting hail or snow where scattering may be enhanced substantially; this effect leads to the bright band which is often observed near the 0°C isotherm on RHI radar displays. Since the effects of snow and hail are, in general, much less severe than those due to rain, the remainder of this paper will emphasize the impact of rain on radar system performance.

Three distinct types of rain merit discussion in this context: convective, stratiform, and orographic. Convective rain usually occurs in cells, i.e., discrete spatial regions, having horizontal dimensions of only a few kilometers. This

type of rain is generally associated with thunderstorm activity which can occur due to local convection on hot summer days or due to the passage of a cold front. These cells may occur in clusters or in bands with regions of no rainfall between the cells. The highest rain rates are generally associated with this type of rain. In contrast, stratiform rain occurs over widespread regions having dimensions on the order of tens of kilometers. Cellular regions of higher rain rate may occur embedded in this light rain rate background; but, nevertheless, the maximum rain rates are usually considerably lower than those found in convective storms. Finally, orographic rain is that rainfall which results from local topographic effects; for example, the lifting of warm air masses over a mountain range may produce orographic rain having characteristics which are quite dependent upon the topography and local climatology. Since the most intense rain rates and, consequently, the most severe electromagnetic interactions are associated with convective cells we will specialize further to this case in the following.

It is well known that rain rate probability distributions vary dramatically over the earth's surface. Nevertheless, it may be argued that the physical processes leading to precipitation, e.g., convection, are fairly universal and, therefore, that one may expect the physical properties of precipitation, cell shape and size, to be reasonably uniform even in different climatic regions. Thus, if this assumption is correct, one may, with care, be able to extrapolate some characteristics of rainfall from one region to another with the understanding that the probability of occurrence may vary drastically.

Convective rain cells typically have horizontal dimensions of only a few kilometers but may be as large as 10-20 km in some cases [2]. The vertical extent of these cells may range up to 20 km; some sample plots of height versus radar reflectivity and equivalent rainfall are shown in Fig. 1.

The cellular nature of such rainfall is exemplified by the 10 GHz PPI display shown in Fig. 2. This figure shows a collection of at least 7 clearly discernible rain cells within a radius of 12 miles of the radar site at Columbus, Ohio, USA, on a July day; several cells having nonsymmetrical shapes and the clear areas between cells can also be noted. Cell orientation as well as orientation between cells tends to show anisotropic characteristics with preferred directions related to the climatology of the region [3]. The spatial inhomogeneity of rainfall can be quite significant as demonstrated by Fig. 3; in this figure two 15 GHz PPI displays of the same rain cell are presented. The first PPI display shows the shape of the cell; and the second contour mode PPI display shows the cell
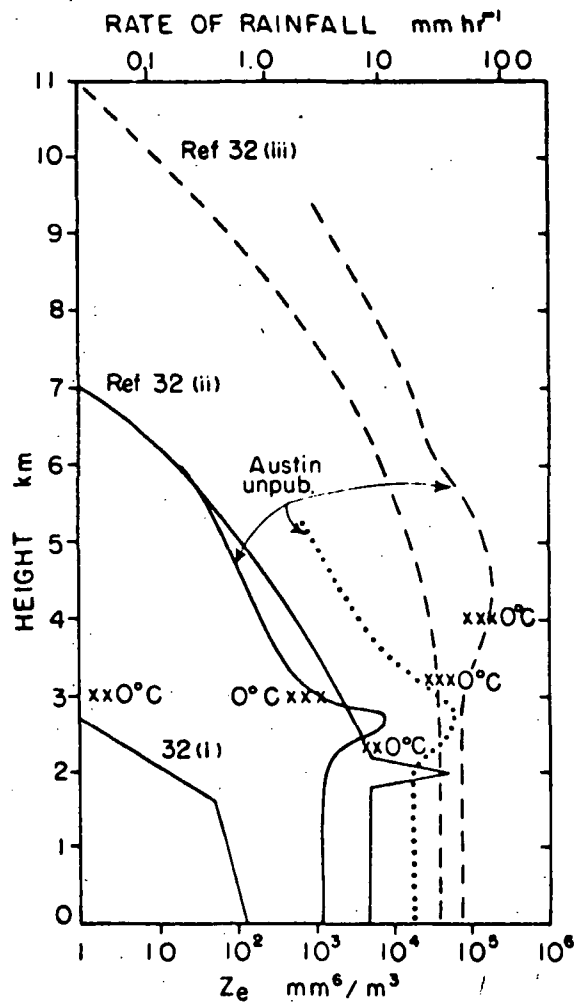
Fig. 1. Height versus radar reflectivity and equivalent
          rainfall rate (Ref. [2]).

with regions of high reflectivity blanked out. Clearly, the
most intense rainfall is occurring only on the far side of the
cell. The vertical inhomogeneity of rain is demonstrated by
Fig. 4; this figure presents a series of vertical 15 GHz
A-scope displays as a raincell passes over the radar site.
Significant reflectivity is observed before the rain actually
reached the ground; and about six minutes later distinct layers
are observed. Finally, the severe attenuation encountered at
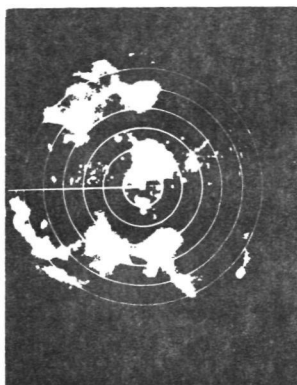15 GHz in heavy rainfall can be noted.

Fig. 2. 10 GHz PPI display showing at least seven clearly
discernible rain cells in Columbus, Ohio, USA. The
range rings are at 2 mile intervals. The small
discrete echoes are ground clutter.

If one averages horizontal cell dimensions over a number of
cells it is found that the average cell diameter tends to de-
crease with increasing rain rate, i.e., cells having low rain
rates may be rather large while the effective diameters of cells
having extremely high rain rates tend to approach an asymptotic
value of about 2 Km. The typical lifetime of convective rain
cells is on the order of one-half to one hour; the decaying cell
may be, however, replaced by a new cell in close proximity to
the original cell.

The water drops that make up rainfall tend to have char-
acteristic shapes as shown in Fig. 5; the smaller drops tend
to be spherical while the large drops flatten in the direction
of motion and the largest drops form a shallow concavity in
the leading surface. It is this lack of symmetry which leads
to polarization dependent attenuation and scattering. The
number of drops per unit diameter per unit volume, $N(D)$, can be
described for our purposes by the Marshall Palmer drop size
distribution [5,6]:

$$N(D) = N_0 e^{-\Lambda D} \quad [\text{drops/m}^3 \cdot \text{cm}]$$

where

$\Lambda = aR^b$
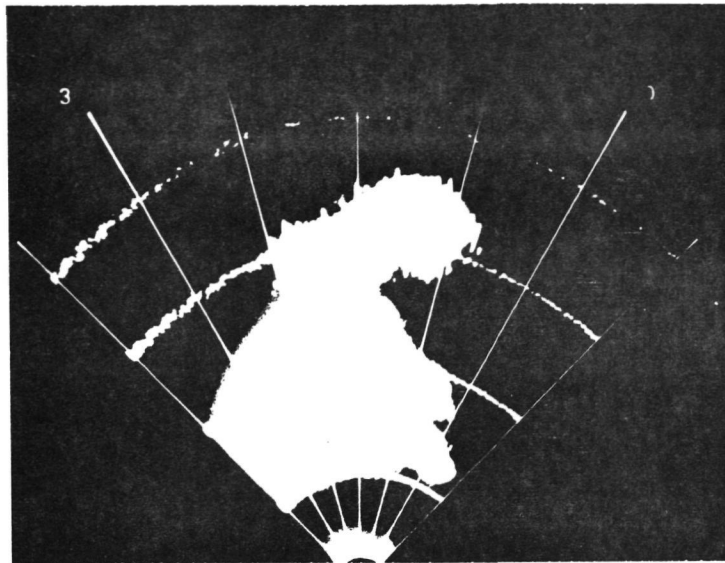$N_0 = 8 \times 10^4$
$a = 41 \ [\text{cm}^{-1}]$
$b = -0.21$

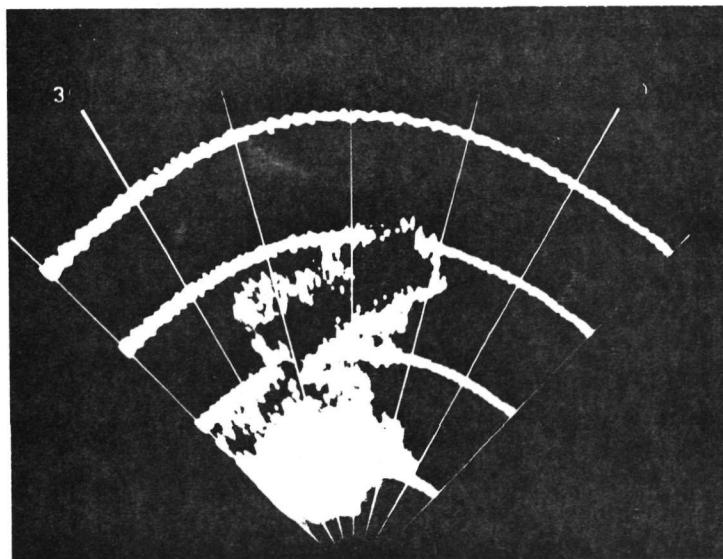Fig. 3a.   15 GHz PPI display of a single rain cell (2 mile range marks.

Fig. 3b.   PPI display one minute later than Fig. 3a with region of high reflectivity blanked out.
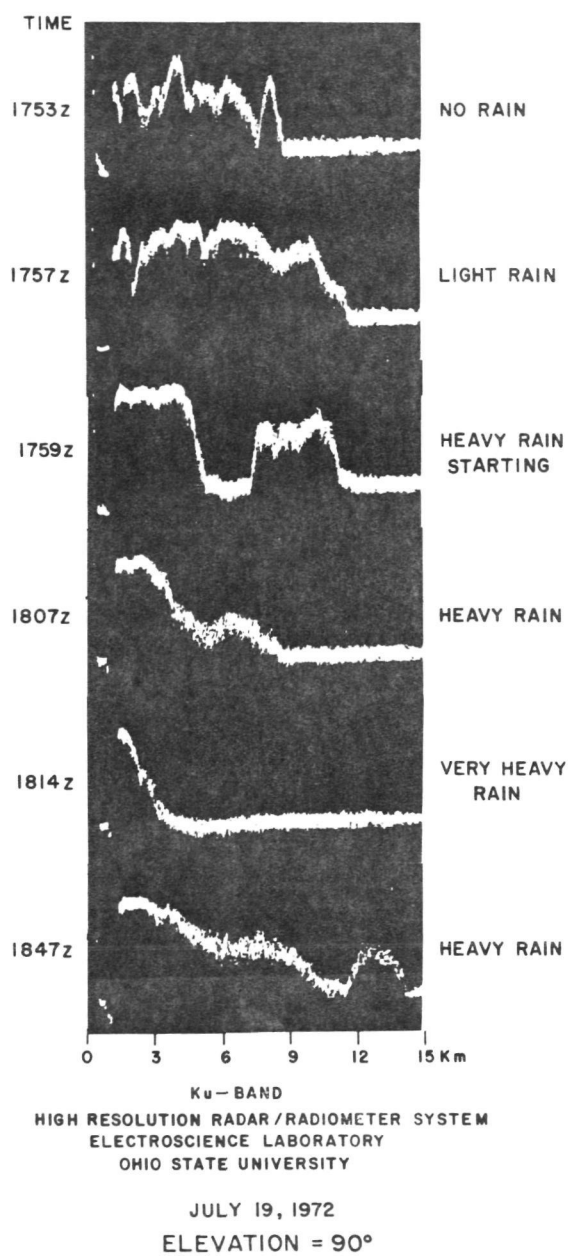
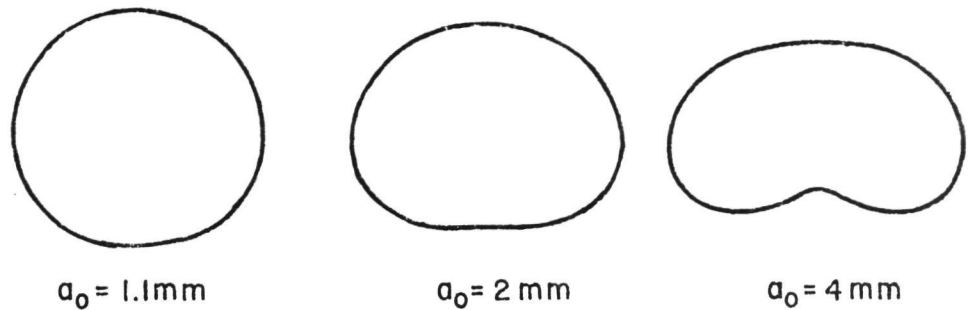Fig. 4. 15 GHz vertical A-scope displays as rain cell passes over radar site.

$a_0 = 1.1$ mm $a_0 = 2$ mm $a_0 = 4$ mm

Fig. 5. Characteristic rain drop shapes for drops with
          rotational symmetry (Ref. [4]). (a_0 = radius of
          sphere having equal volume.)

and D is in centimeters and R in mm/hr. This distribution is
shown in Fig. 6 for various rain rates; it can be noted that
drop sizes larger than 5 mm are extremely rare. As the rain
rate increases, the number of large drops increases; and these
electrically large drops tend to dominate the electromagnetic
interactions. It is of interest to note that the liquid water
content of rainfall is normally much less than the equivalent
liquid water content of the water vapor contained in even a
normal dry day as shown in Fig. 7. The parameter rain rate is
used widely in describing precipitation since it is a quantity
which is easily measured at the surface of the earth. This
parameter can, however, be misleading since rain drops may be
carried upward within a rain cell due to strong updrafts;
therefore, this parameter must be used with a degree of caution.

The relative dielectric constant and loss tangent of liquid
water are shown in Figs. 8 and 9 [7]. Thesy curves show a
rather marked temperature dependence which tends to be masked
by other factors when attenuation and scattering calculations
are performed. We also observe that the loss tangent is large
over the frequency range of roughly 10 to 100 GHz.

The presence of these dielectric drops along the propaga-
tion path of an electromagnetic wave gives rise to a number of
resultant effects as shown pictorially in Fig. 10. These
effects include; attenuation, dispersive phase shift, de-
polarization, change in angle of arrival, backscatter, and
noise emission. The attenuation results from both absorption
and scattering loss and may be expressed as

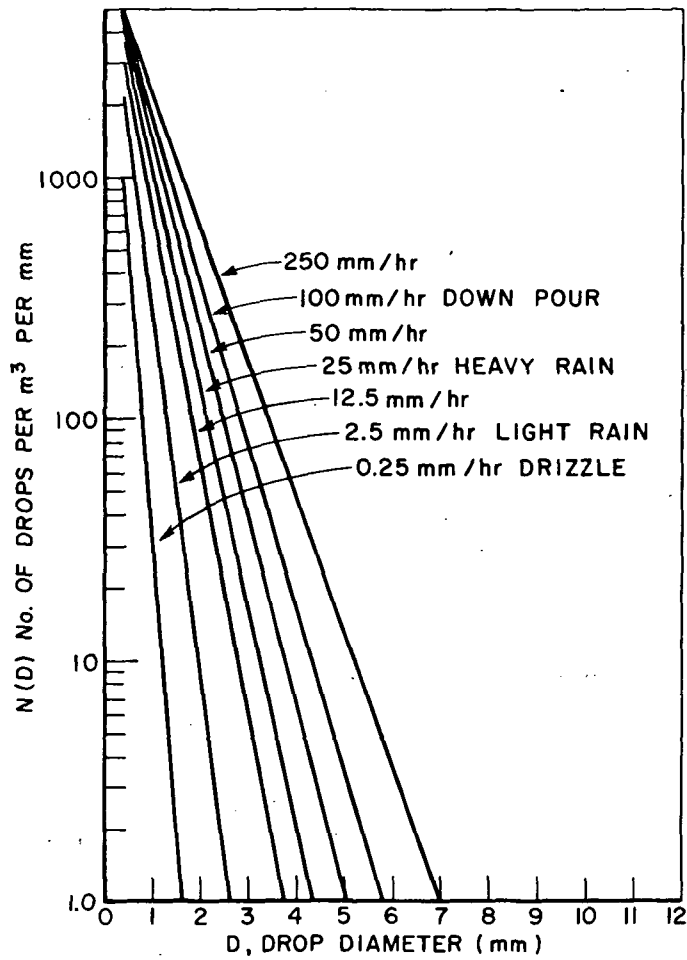$$\alpha_t = \alpha_a + \alpha_s \quad [\text{dB/Km}]$$

Fig. 6. Drop size distributions.

where

α_t = total attenuation rate

α_a = rate of attenuation due to absorption

α_s = rate of attenuation due to scattering

and either attenuation rate is given by
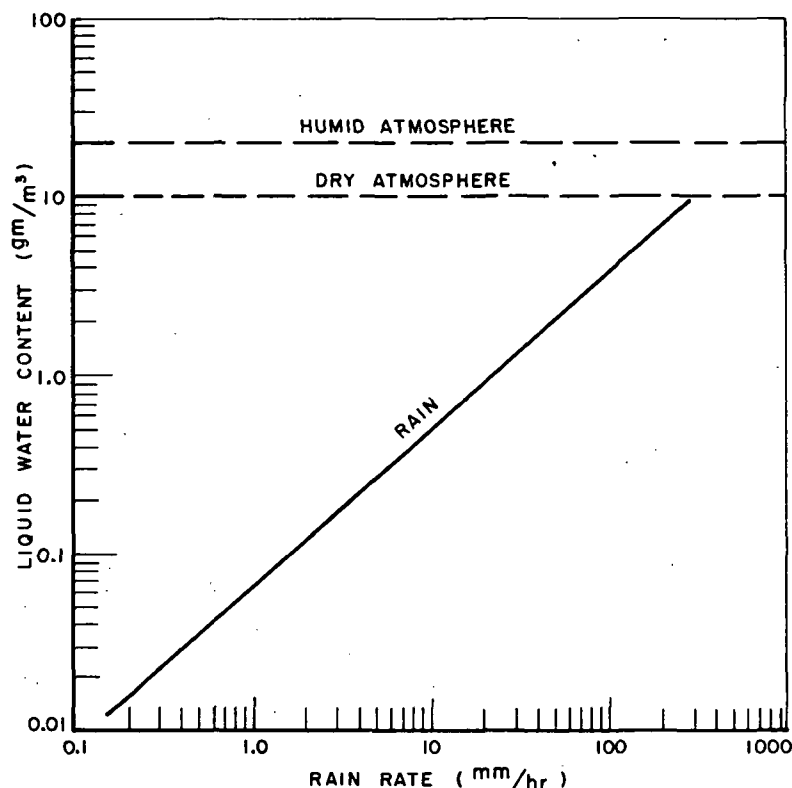
$$\alpha_i = 4.343 \int_0 Q_i(D)N(D)dD.$$

Fig. 7. Equivalent liquid water content of rainfall and
water vapor for typical dry and humid atmospheres.

Here, Q_i is either the absorption or total scattering cross
section of a drop of diameter D [8]. These cross sections are,
of course, dependent upon frequency as well as the drop tempera-
ture and drop size. Plots of these attenuation rates are given
in Fig. 11 for various rain rates; these calculations were based
upon the Marshall Palmer drop size distribution, Stogryn's
dielectric constant, and the Mie cross sections for spherical,
lossy dielectric drops. For low rain rates and/or low fre-
quencies the dominant effect is that of absorption; however,
for higher frequencies and/or higher rain rates scattering loss
can become significant. This characteristic is emphasized by
the plot of albedo, i.e., the ratio of scatter loss to total
attenuation, shown in Fig. 12; the albedo approaches 0.5 for
high frequencies and high rain rates just as the albedo of a
single large drop approaches 0.5 with increasing size. The
attenuation rate is plotted along with the attenuation rates
due to fog and atmospheric gases in Fig. 13; this figure in-
dicates that attenuation due to rain may be as much as an
order of magnitude higher than that encountered in either fog
or clean air at most frequencies of interest. This rain at-
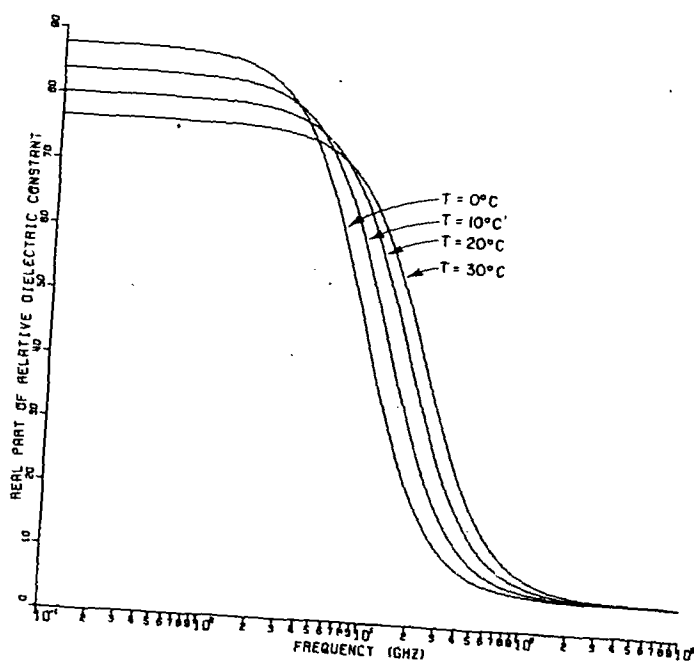
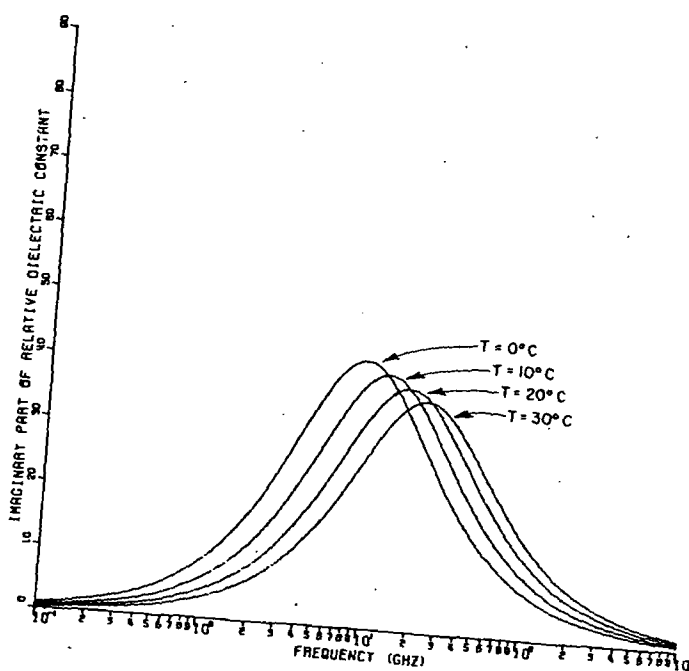Fig. 8a. Real part of the relative dielectric constant of liquid water.

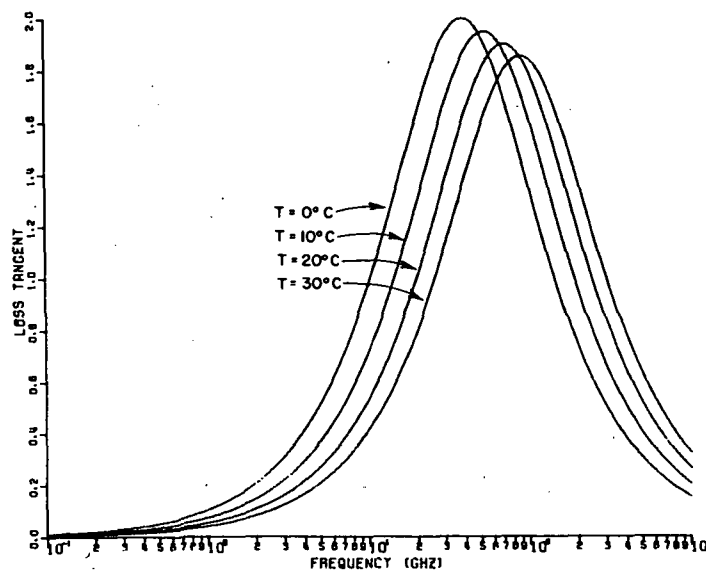Fig. 8b. Imaginary part of the relative dielectric constant of liquid water.

Fig. 9. Loss tangent for liquid water.

tenuation is produced by spatially inhomogeneous rain cells passing through the propagation path; and, thus, the total path attenuation may vary rapidly with time. Fading rates as rapid as 1/8 dB/sec were encountered, for example, on a 15.3 GHz earth-satellite propagation path [10].

Since the rain filled atmosphere is a lossy medium, thermodynamic arguments indicate that the medium itself must emit noise. For sufficiently narrow beam antennas, the observed radiometric noise emission may be related quite simply to the total path attenuation by

$$T_s = T_m (1-10^{-A/10}) \quad [°K]$$

where T_s is the radiometric sky temperature, T_m is the mean absorption temperature of the medium, and A is the total path attenuation expressed in decibels [11]. The measured correlation between radiometric sky temperature and total path attenuation for a 15.3 GHz earth-space propagation path is shown in Fig. 14. Note that these radiometric sky temperatures do not exceed the mean absorption temperature and, thus, do not present a problem in system design since much higher noise levels are generated in current receiver front ends. Nevertheless, this noise emission provides a very useful means of detecting the presence of rain and indirectly measuring total path attenuation.
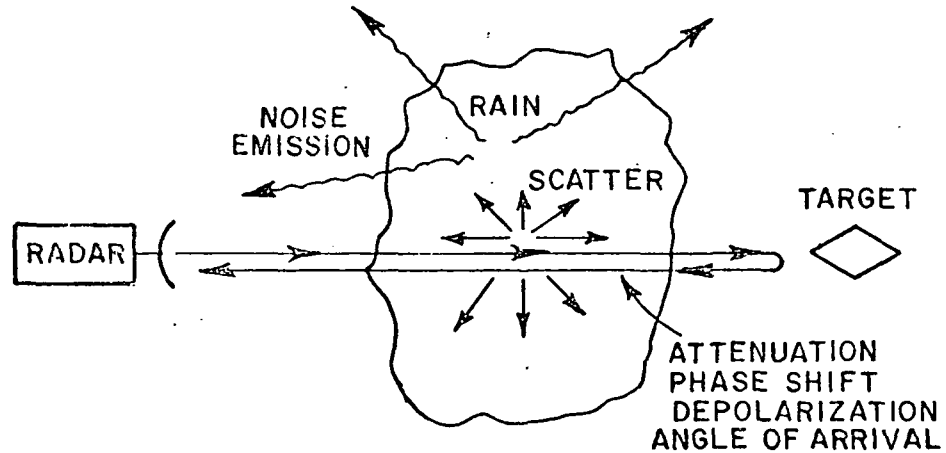
Fig. 10.   Interactions between an electromagnetic wave and rain.

It has already been pointed out that scattering produces attenuation; in addition, the energy backscattered to the radar produces a radar return, i.e., clutter. The radar range equation for this clutter case is

$$P_{RCVD} = \frac{\lambda^2 G \, c \, \tau \, P_{TRANS}}{2^7 \, \pi \, r^2} \cdot \eta$$

where λ is the wavelength, G is the radar antenna gain, c is the velocity of propagation, τ is the radar pulse length, r is the range to the scattering volume, η is the volumetric radar cross section of the rain, and P_{TRANS} and P_{RCVD} are the transmitted and received powers, respectively [12]. The r^2 range dependence is a consequence of the assumption that the radar resolution cell is filled with rain. The volumetric radar cross section is given by

$$\eta = \int_0^\infty \sigma(D) N(D) dD$$

where σ is the usual radar backscatter cross section of a single rain drop of diameter D; η is plotted in Fig. 15 for various rain rates. The calculation of the volumetric radar cross sections shown in Fig. 15 were based on the same assumptions as those noted earlier for the attenuation calculation shown in Fig. 11. This radar backscatter signal is produced by scattering from many randomly spaced rain drops; consequently, the signal varies randomly about a mean value
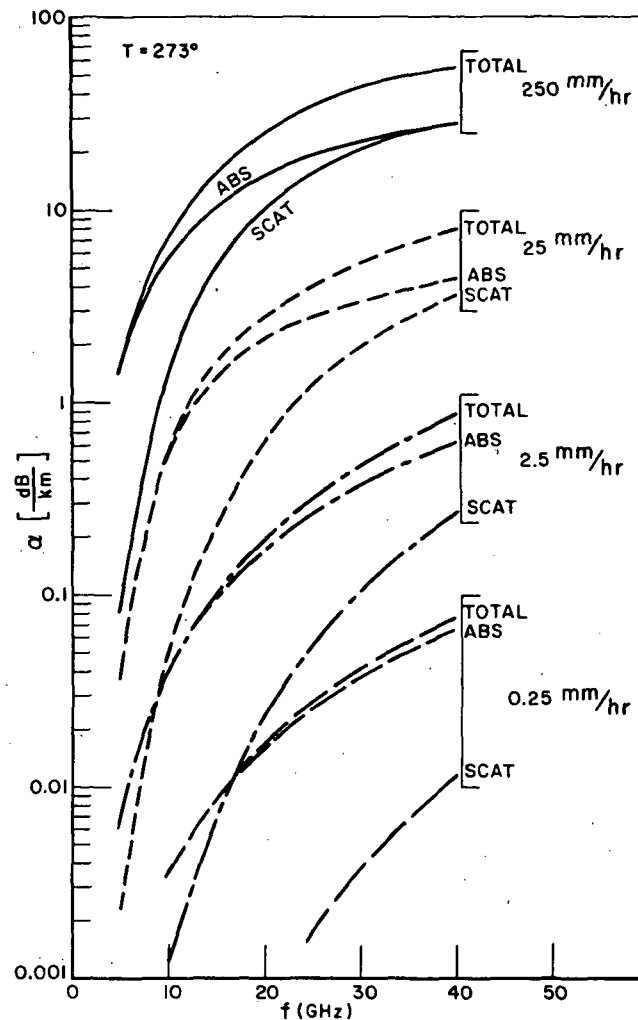
14

Fig. 11. Attenuation rates in rain.

as the relative positions of the drops change. The time to in-
dependence, i.e., the time required for the drops to rearrange
themselves so that an uncorrelated signal is produced, is on the
order of milliseconds to tens of milliseconds for typical radar
frequencies [13].

As a wave propagates through rain it suffers a phase shift
in addition to the attenuation described earlier. This phase
shift may be calculated using the methods of Van du Hulst [14].
Phase shifts calculated in this manner are shown in Fig. 16 [15].
These phase shifts are recognized to be comparable or, in some
cases, less than the phase shifts produced by the atmospheric
gases in clear air [16]. However, it may be that the inhomo-
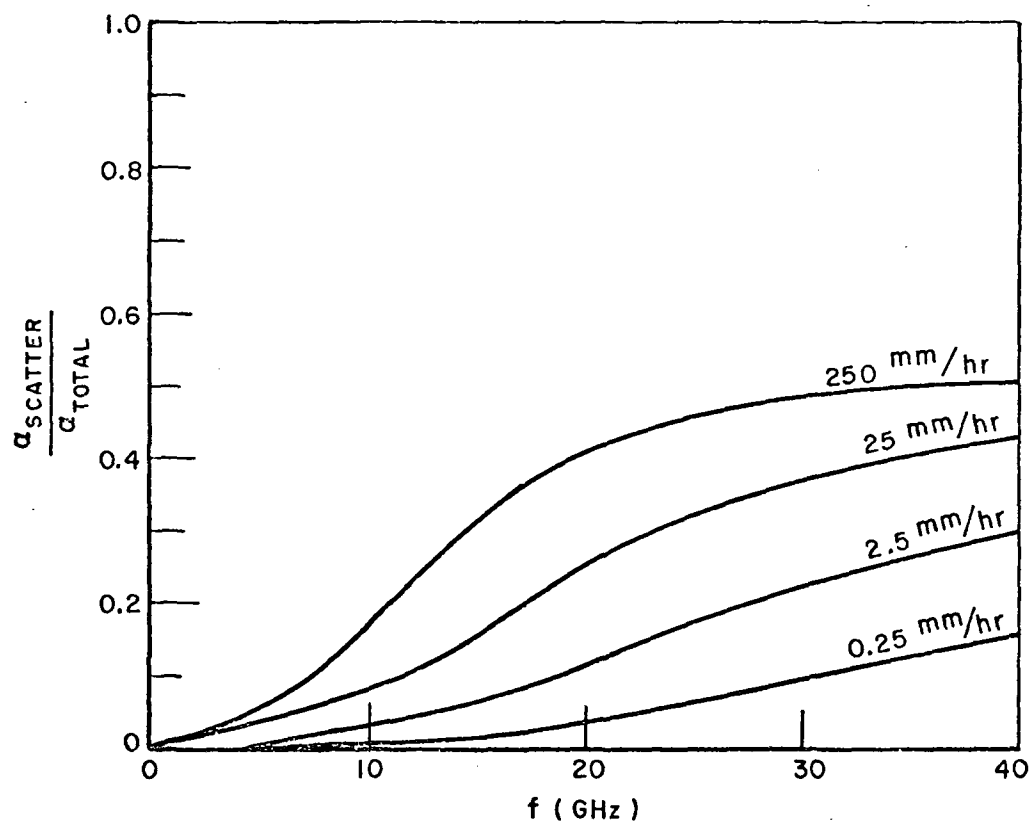geneity of the rainfall within the illuminated region may

Fig. 12. Albedo as a function of rain rate and frequency.

produce nonuniform phase shifts and attenuation across the beam which, in turn, may alter the direction of propagation. There is very little data available at the present time concerning these effects.

It was noted earlier that nonspherical drop shapes produce depolarization. These effects are discussed in considerable detail in another paper presented at this meeting [17]. Let it suffice here to simply indicate the magnitude of this problem in intense rain; in this case, differential attenuations as high as 5 dB/Km, differential phase shifts as large as $\pm$20 deg/Km, and cross polarization coupling exceeding -20 dB may be encountered between orthogonal linear polarizations [18].

The preceding discussion has indicated the nature of the interactions between propagating electromagnetic waves and rain. These effects are reasonably well understood and their gross influence on system performance may be estimated. In most cases, however, little information is available concerning the likelihood of occurrence of these effects. This is largely due to
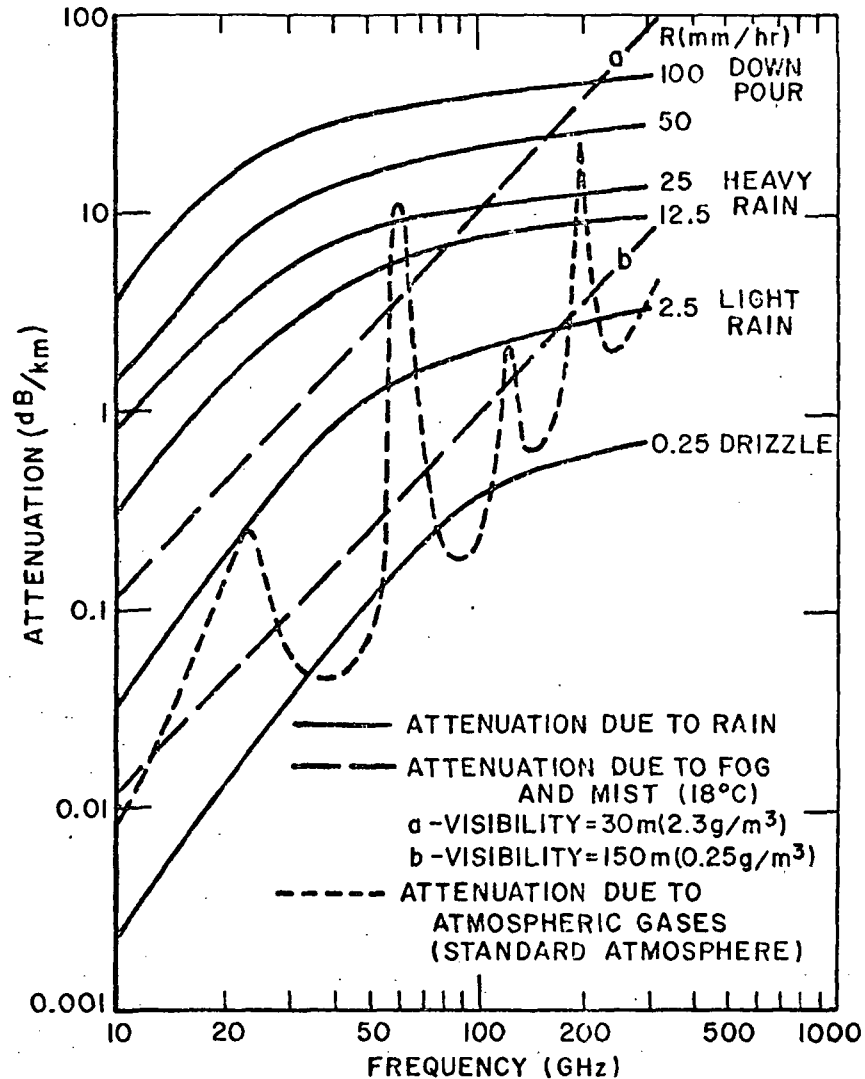
Fig. 13. Comparison of attenuation due to atmospheric gases,
          rain, and fog (Ref. [9]).

the lack of data describing the fine scale temporal and
spatial statistics of rainfall and the dependence of these
statistics on climatic region. Current and future communi-
cation link experiments will certainly shed light on some of
these questions if care is exercised in the extrapolation of
the results to the radar case. For example, it is necessary to
categorize propagation paths into four classes depending upon
whether a single rain cell or multiple rain cells are likely
to be encountered on the path and whether the path is a
terrestrial path influenced only by horizontal variations in
rainfall or an earth-space path influenced by both horizontal
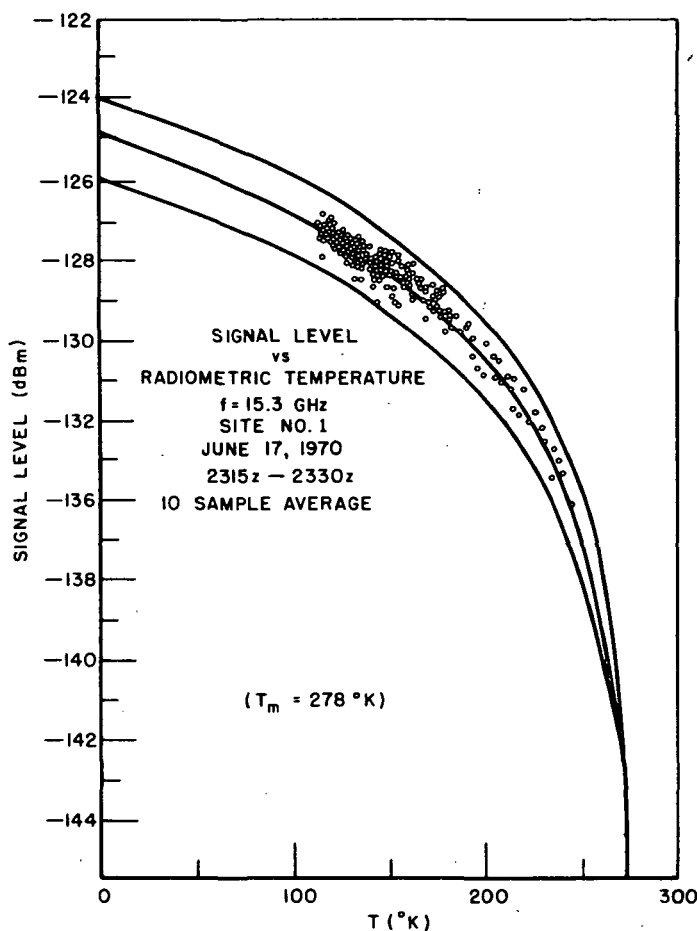and vertical spatial rainfall variations.

Fig. 14. Comparison of rain attenuation and radiometric sky
temperature.

REFERENCES

[1] IURCUM Colloquium on the Fine Scale Structure of
Precipitation and Electromagnetic Propagation, Nice,
France, October, 1974. Entire proceedings contained in
Journal de Recherches Atmospheriques, v. 8, No. 1-2, 1974.

[2] "The Structure of Precipitation Systems - A Review,"
T. W. Harrold and P. M. Austin, Journal de Recherches
Atmospheriques, v. 8, No. 1-2, p. 41, 1974.

[3] "Radar Measurements of Site-Diversity Improvement During
Precipitation," J. I. Strickland, Journal de Recherches
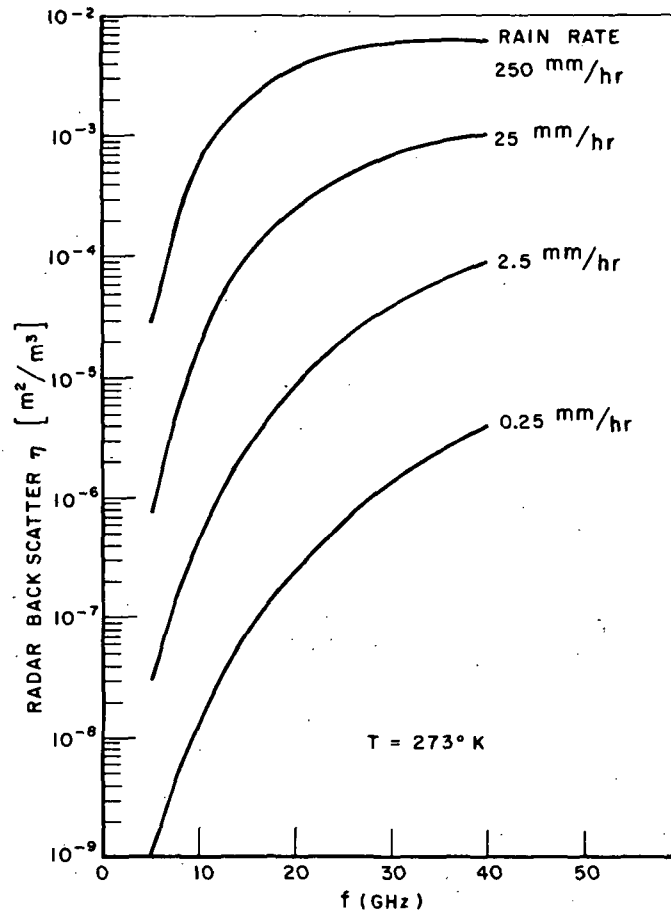Atmospheriques, v. 8, No. 1-2, p. 451, 1974.

Fig. 15. Volumetric radar backscatter cross section of rain.

[4] "A Semi-Empirical Determination of the Shape of Cloud
and Rain Drops," H. R. Pruppacher and R. L. Pitter, Jour.
Atmospheric Sci., v. 28, p. 86, 1971.

[5] "The Distribution of Raindrops with Size," J. S. Marshall
and W. M. Palmer, Jour. of Meteorology, v. 5, p. 165, 1948.

[6] "The Cloud Physics of Particle Size Distributions - A
Review," R. C. Srivastava, Journal de Recherches
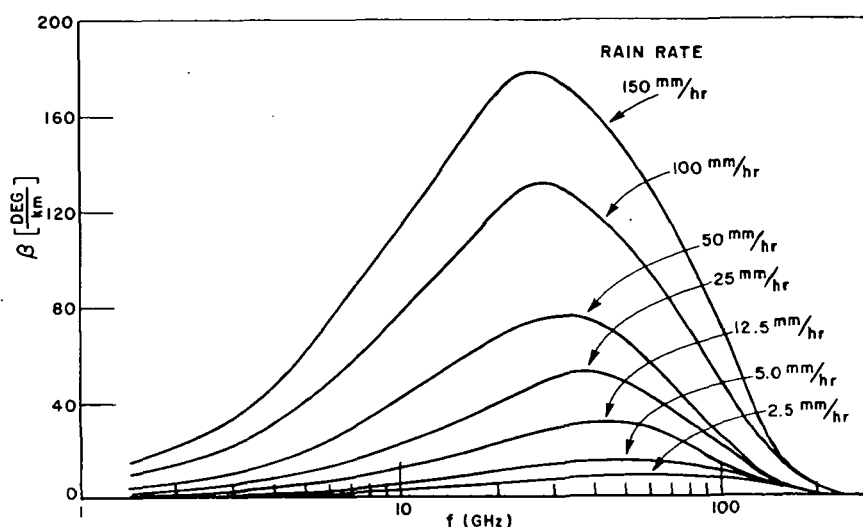Atmospheriques, v. 8, No. 1-2, p. 23, 1974.

Fig. 16. Phase shift due to rain.

[7] "Equations for Calculating the Dielectric Constant of Saline Water," A. Strogyn, IEEE Trans., v. MTT-19, p. 733, 1971.

[8] "Propagation of Short Radio Waves," D. E. Kerr, Dover, p 445, 1951.

[9] "Atmospheric Effects of Millimeter Wave Communication Channels," E. Mondre, NASA Goddard Space Flight Center, Rept. X-733-70-250, March, 1970.

[10] "A 15.3 GHz Satellite-to-Ground Path-Diversity Experiment Utilizing the ATS-5 Satellite," D. B. Hodge, Radio Science, v. 9, p. 1, 1974.

[11] "Rain Attenuation at 15 and 35 GHz," K. N. Wulfsberg and E. E. Altshuler, IEEE Trans., v. AP-20, p. 181, 1972.

[12] "Introduction to Radar Systems," M. I. Skolnik, p. 539, McGraw-Hill, 1962.

[13] "Advances in Radar Meteorology," D. Atlas, p. 404 in "Advances in Geophysics," H. E. Landsberg and J. Van Mieghem, Vol. 10, Academic Press, 1964.

[14] "Light Scattering by Small Particles," H. C. Van du Hulst, p. 31, Wiley, 1957.

[15] "Computed Transmission through Rain at Microwave and Visible Frequencies," D. E. Setzer, Bell Sys. Tech. Jour., v. 49, p. 1873, 1970.

[16] "Transit-Time Variations in Line-of-Sight Tropospheric Propagation Paths," D. A. Gray, Bell Sys. Tech. Journ., v. 49, p. 1059, 1970.

[17] "Some Polarization Effects for Millimeter Wave Propagation in Rain," W. Vogel, NATO Advanced Study Institute, Goslar, Germany, September 22-October 3, 1975.

[18] "Differential Attenuation and Differential Phase Shift of Radio Waves due to Rain: Calculations at Microwave and Millimeter Wave Regions," T. Oguchi and Y. Hosoya, Jour. de Recherches Atmospheriques, v. 8, No. 1-2, p. 121, 1974.